# Pulsed Electrochemical Synthesis and Characterization of Tin Sulfide-Tin Dioxide Nanocomposites

*Hassan Karami[1,2,\*], Somayyeh Babaei[1], Sara Matini[1]*

[1]Nano Research Laboratory, Department of Chemistry, Payame Noor University, Abhar, Iran
[2]Department of Chemistry, Payame Noor University, 19395-4697, Tehran, I.R. of Iran
[\*]E-mail: karami_h@yahoo.com

In this paper, tin sulfide-tin dioxide nanocomposites were synthesized by the pulsed-current electrochemical method on the surface of tin substrate in $Na_2S$ solution. To obtain uniform morphology, narrowest size distribution, and the best composition of sample, the effects of experimental variables such as sodium sulfide concentration, types and concentration of synthesis additives, pH, bath temperatures, pulse frequency, and pulse height (current amount) are investigated and optimized. The prepared samples are characterized by scanning electron microscopy (SEM), transmission electron microscopy (TEM), and X-ray diffraction (XRD) techniques. The optimized conditions include 92 $mA.cm^{-2}$ current density, 13 Hz pulse frequency, 0.008 M sodium sulfide, pH 12.5, and 25 °C electrocrystallization temperature. In optimum conditions, uniform SnS-SnO2 nanocomposite in orthothombic nanorod form with 30 nm average diameter and 200 nm average length are synthesized.

## 1. INTRODUCTION

During last decade, nanomaterials have attracted much attention in various fields of science and technology [1-2]. The nanostructured materials were synthesized by a variety of physicochemical methods, including metal evaporation [3], spray pyyrolysis [4], sol-gel [5] and electrochemical methods [6]. The electrosynthesis of nanomaterials has received a great deal of attention in the past several years. This is probably because electrochemical synthesis methods is a low cost and the reaction conditions in these methods that can be carried out under mild conditions and the properties of nanoparticles can be controlled by several parameters such as current density, applied potential, reaction temperature, and solution composition. In the recent years, a lot of nanostructures have been synthesized by the electrochemical methods such as cyclic voltammetry [7-10], potentioastatic [11-15],

galvanostatic [16-17], and pulsed-current [18-22] methods. Compared with conventional galvanostatic method, pulse galvanostatic method is a modified, simple, and controllable method. In the pulsed-current method, nanostructured materials can be synthesized on the electrode surface by controlling pulse variables such as pulse height (current density), pulse time, and relaxation time. There are many reports which show that the pulsed- current electrosynthesis is more efficient than the direct current [23-26].

SnS and $SnO_2$ are two important IV-VI group semiconductors, with a band gaps 1.48 (or smaller) and 4.08 eV (or smaller), respectively. Different morphologies can play roles in the properties. They include nanoparticles [27-30], nanostructures [31], nanoholes [32], nanorods [33], nanoplanes [34], nanowires [35-37], nanodiscs [38-40], and orthorhombic structures [41]. All can be prepared by different methods, such as solvothermal [42], vapor deposition [43-48], electrochemical deposition [49-51], aqueous solution methods [52], and spray pyyrolysis [53]. Tin sulfide and tin dioxide nanoparticles have wide applications in many fields such as solar cells, lithium ion batteries, semiconductors, photocatalysts, photovoltaic materials, and also as gas- sensing agents in the solid-state sensors [54-56].

There are a few reports about using SnS and its composites as a gas- sensing agent. Huang et al. prepared porous flower-like tin oxide ($SnO_2$) nanostructure by annealing of the flower-like tin sulfur ($SnS_2$) nanostructures [57]. These $SnO_2$ nanostructures exhibit a good response and reversibility to some organic gases, such as ethanol and *n*-butanol. In addition, the sensor exhibit a good response to methanol, 2- propanol, and acetone.

Park et al. fabricated $NO_2$, $NH_3$, and xylene gas sensors using mixed $SnO_2$ nanoparticles with 1 %wt MWCNTs sensing materials on micro-platforms [58]. The fabricated gas sensors were characterized to $NO_2$, $NH_3$, and xylene gases, respectively, as a function of concentration at 300 ºC, and temperature from 180 ºC to 380 ºC at constant concentration. From these results, mixed $SnO_2$ nanoparticles with 1 %wt MWCNTs showed good sensitivity and selectivity at low power operation below 30 mW. Authors noted that the fabricated micro-gas sensors could be used for ubiquitous sensor network applications to monitor environmental pollutants in the air.

Zhang et al. prepared SnS nanoparticles through directly dispersing melted tin in a sulfur-dissolved Solvent [59]. The as-prepared SnS nanoparticles display novel blue-UV emission, promising for applications in optical devices.

Comini et al. presented tin oxide nanobelts based gas sensor with a simple DC-resistive measurement in 2002 [60]. A platinum interdigitated electrode was made using sputtering technique with shadow masking on alumina substrate. Then, a bunch of nanobelts was transferred onto the electrodes for electric conductance measurements, the gases tested were CO, $NO_2$, and ethanol that are important for environmental applications, for breath analyser and food quality control. CO and ethanol were found to increase the conductivity that is common for an *n*-type semiconductor such as tin oxide.

Another work on $SnO_2$ 1D nanostructure, reports the effect of catalysts on nanowires sensing properties [61]. Nanobelts and nanowires were mixed with CuO. This catalyst was chosen since it is known in thick and thin film to enhance the sensing properties towards $H_2S$ of $SnO_2$ (an effect ascribed to the p–n junction formation). The increase in $H_2S$ response was confirmed in 1D nanostructure, the

detection limit reached was lower than 3 ppm. Of course the addition of a polycrystalline material reduces the advantages of the use of single crystalline metal oxide as sensing layer.

Yu et al. recently published a contribution on tin oxide nanobelts proving their integration with micro-machined substrate [62] which is crucial if a real application is envisaged, and showing their sensitivity to nerve agent, an application of increasing interest for security reasons.

In this work, we describe pulsed-galvanostatic method to synthesize tin sulfide-tin dioxide nanocomposites with different morphologies such as nanoparticles and nanorods. A series of experiments were conducted to establish the optimum conditions to obtain uniform morphology, narrowest size distribution, and best composition of the nanocomposite by the "one at a time" method. An optimized $SnS$-$SnO_2$ nanocomposite sample was used to construct a solid- state sensor to detect oxygen gas.

## 2. EXPERIMENTAL

### 2.1. Materials

Sodium sulfide ($Na_2S$), copper (II) sulfate ($CuSO_4$), and acetone were purchased from Merck and were used without any purification. Sodium dodecyl sulfate (SDS), polyvinyl pyrrolidone (PVP), glycerol, and cetyltrimethyl ammonium bromide (CTAB) were purchased from Fluka and Aldrich. Pure tin substrate was prepared from the national iranian Simaran company. Double-distilled water was used in all experiments.

### 2.2. Instrumental

The morphologies, Particles sizes and the compositions of samples were characterized by the scanning electron microscopy (SEM, Philips, XL-30, and The Netherlands). A transmission electron microscope (TEM, Zeiss EM900, 80 keV) was used to measure the size and shape of particles accurately. X-ray powder diffraction (Philips X'pert diffractometer using Cu [(K$\alpha$)] radiation with $\lambda$= 0.15418 nm) was used to determine the composition of the samples. MPS-3010L model of a power source, made by the Taiwan Matrix company was used for making a constant current. A home-made electrical pulse apparatus was applied to make the reproducible current pulses. The temperature of the synthesis solution was controlled by circulator (HAKKEL model), made by Fisons company (Germany).

### 2.3. Procedures

#### 2.3.1. Electrode preparation

In order to make tin electrodes, pure tin was melted in $400^{\circ}C$ and was cast in a steel mould. The structure of the electrode which obtained by the casting method is shown in Fig.1.
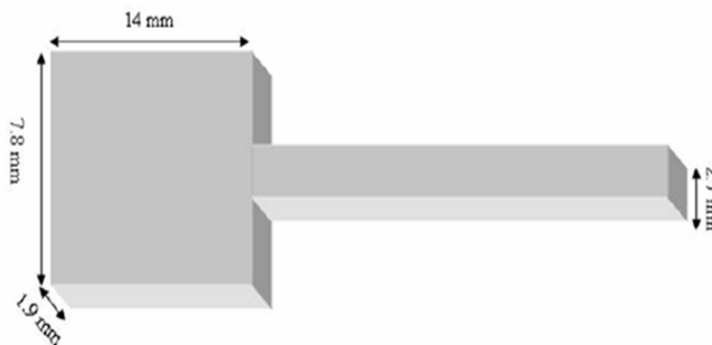
**Figure 1.** Scheme and dimensions of the used electrode.

*2.3.2. Synthesis procedure*

Before each deposition, the tin electrodes were placed in the 35 %wt $HNO_3$ for 30 s and then rinsed with double-distillated water to remove any surface oxidized species in contact with air. Two stainless steel cathodes coupled with the prepared tin electrode as anode of the electrochemical cell. The electrodes were put in the synthesis solution including 0.008 M $Na_2S$, and temperature of 25 °C. The pH of synthesis solution was adjusted at 12.5 by adding NaOH solution. By applying current pulse, $SnS$-$SnO_2$ nanocomposites were directly synthesized on the surface of tin electrode (anode) by oxidation of the tin substrate and combination of $Sn^{2+}$ with sulfide and hydroxide ions to form $SnS_2$ and $Sn(OH)_4$ in composite form. Finally, $Sn(OH)_4$ was dehydrated to $SnO_2$ and the $SnS$-$SnO_2$ nanocomposite was formed.

In the presented method, there are some effective parameters such as sodium sulfide concentration, pH, type and concentration of additives, solution temperature, pulse frequency, and pulsed current amplitude which can change the morphology, particles sizes, and the composition of the synthesized samples. The resulted precipitates were filtrated, washed two times with double-distilled water, then with acetone, and finally were dried in an oven at 80 °C for 20 min. The amounts of synthesis parameters were varied and optimized by the "one at a time" method to obtain a sample with the best particle size and morphology. The morphology and particles sizes of the samples were characterized by SEM and TEM. XRD patterns (using Cu [$(K_\alpha)$] radiation with $\lambda = 0.15418$ nm) were used to determine the composition of the samples.

## 3. RESULTS AND DISCUSSION

*3.1. Pulse specifications*

Tin sulfide-tin dioxide ($SnS$-$SnO_2$) nanocomposites were directly synthesized by the pulsed current method on the surface of tin electrode in a synthesis solution including 0.008 M sodium sulfide, solution pH of 12.5, electro-crystallization temperature of 25 °C, pulse current of 92 mA.cm$^{-2}$, pulse frequency of 13 Hz. In the current study, a direct current with constant amplitude was supplied by a common power supply instrument. The output of the power supply system (DC current) was

connected to a home-made pulse maker apparatus. The current output of the pulse system is a pulsed current as it has been previously explained [63]. There are 4 variable parameters for pulse system including pulse height, pulse time, relaxation time and pulse frequency. The results of our initial experiments indicated the desirability of relaxation time/pulse time ratio of 3 for majority of syntheses. Therefore, the ratio of 3 was selected for further experiments. At a constant ratio of relaxation time to pulse time, a pulse system has 3 variable parameters including pulse height, pulse time, and pulse frequency. In the present method, there are some parameters, such as pulse current, pulse frequency, concentration of sodium sulfide, pH, and temperature of synthesis solution which their amounts optimized by the "one at a time" method. The synthesized samples were characterized by SEM, TEM, and X-ray diffraction (XRD). The following sections of this paper describe the optimization experiments of the other parameters.

After optimization of synthesis conditions, the $SnS-SnO_2$ nanocomposite was used as an oxygen gas-sensing agent to construct a new solid-state sensor. This sensor ability for measurement of the different gases, such as $NH_3$, $O_2$, $H_2O$, CO, $H_2$, and LPG was investigated. Variation in the sensor resistance was used as optimizing signal. Among the cited gases, the constructed sensor showed a high dynamic range, high sensitivity, and short response time to oxygen without any considerable interference of the other gases.

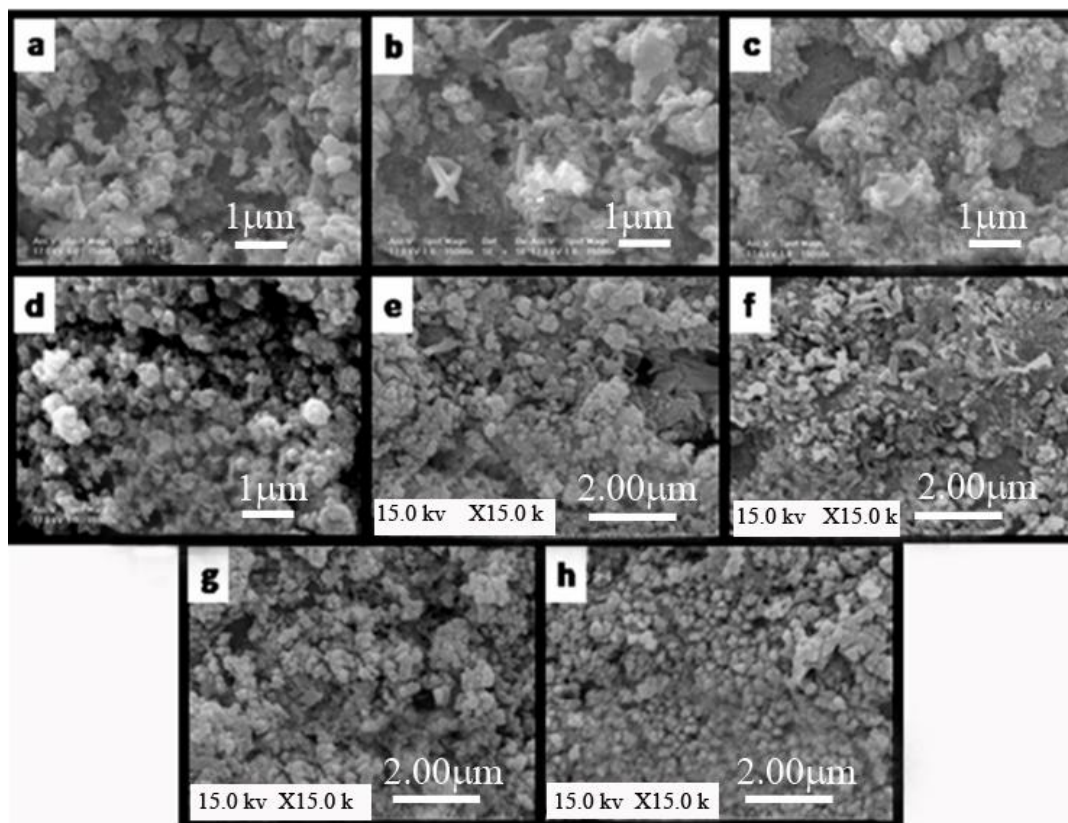*3.1. Optimization of pulsed current amplitude*



**Figure 2.** SEM images of tin sulfide samples synthesized at different pulsed- current amplitudes; 6 mA.cm$^{-2}$ (a), 18 mA.cm$^{-2}$ (b), 37 mA cm$^{-2}$ (c), 61 mA.cm$^{-2}$ (d), 80 mA cm$^{-2}$ (e), 92 mA.cm$^{-2}$ (f), 104 mA cm$^{-2}$ (g), 122 mA.cm$^{-2}$ (h). The other experimental conditions were kept constant.

The effects of pulsed current amplitude were investigated on the morphology and particles sizes of the synthesized samples. The pulse height was varied from 6 mA cm$^{-2}$ to 122 mA cm$^{-2}$, and the other parameters were kept constant (a temperature of 25 °C, pulse frequency of 13 Hz, concentration of sodium sulfide 0.008 M, a pH of 12.5). The obtained samples were studied by SEM images (Fig. 2). As we can see in Fig. 2, any increasing in current amplitude causes a speed-up nucleation of species thus the produced particles will be smaller. The observed effect has been previously reported for electrochemical synthesizing of other nanoparticles [64]. The 92 mA.cm$^{-2}$ pulse current amplitude makes more uniform and smaller nanoparticles than the others. Thus, the amount of 92 mA.cm$^{-2}$ was selected as optimum pulsed current amplitude in SnS nanoparticles synthesis.

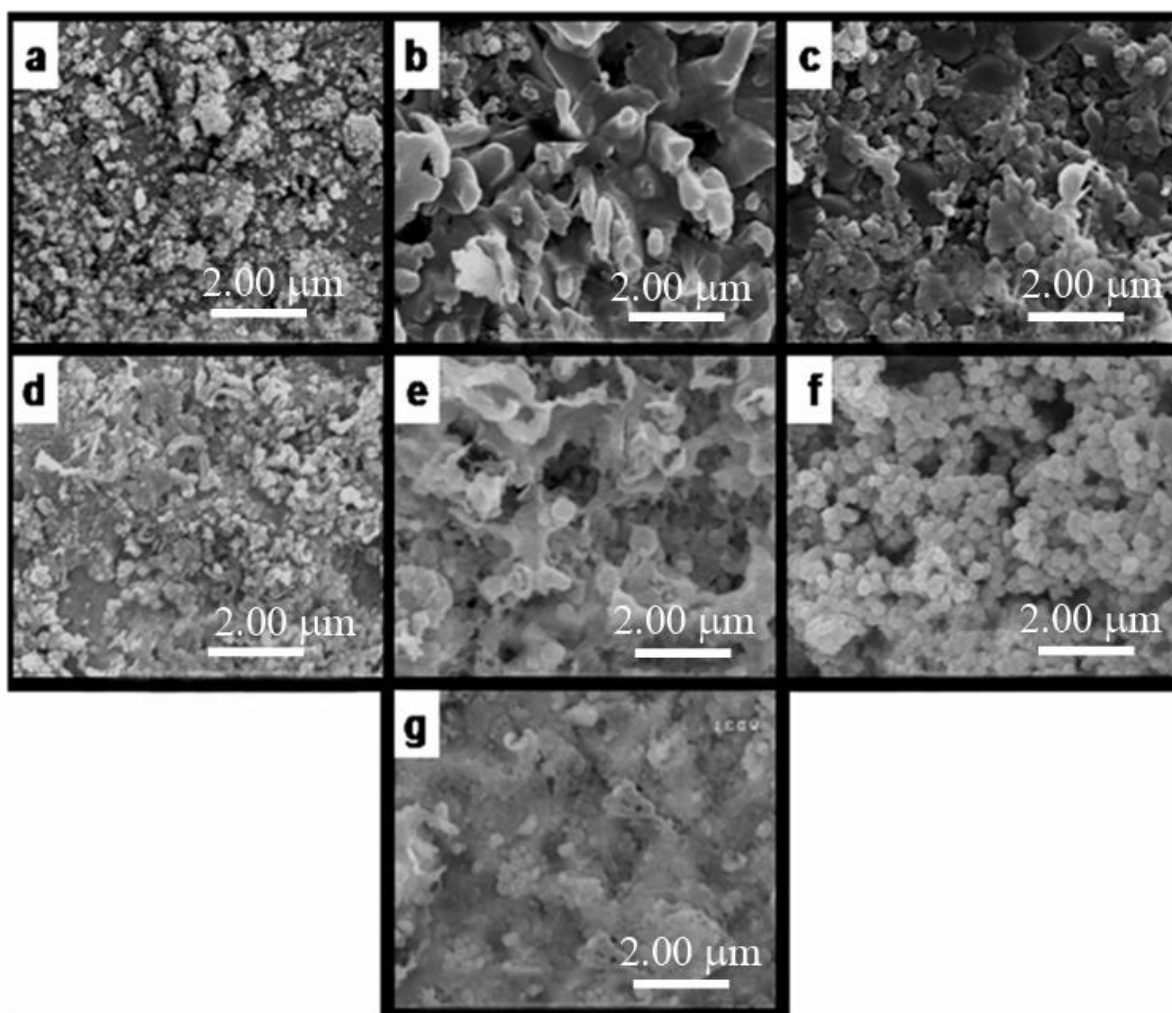*3.2. Optimization of pulse frequency*



**Figure 3.** SEM images of tin sulfide samples synthesized at different pulse frequencies; simple constant current without pulse (a), 4 Hz (b), 7 Hz (c), 10 Hz (d), 11 Hz (e) 13 Hz (f), and 15 Hz (g). The other experimental conditions were fixed.

In the present method, each pulse cycle consists of one pulse time and one relaxation time, and the pulse frequency (f) includes numbers of pulse cycles in the time unit (s). In the current work, the

ratio of relaxation time to pulse time is kept constant of 3 therefore, the pulse time (t on ) and relaxation time (t off ) can be easily calculated from pulse frequency (1 and 2 equations):

(1) $$t_{on}(s) = \frac{1}{4f}$$

(2) $$t_{off}(s) = \frac{3}{4f}$$

To investigate the effects of pulse frequency on the morphology and particles sizes of the synthesized nanocomposite samples, we varied the amount of this parameter from 0 to 15 Hz while the amounts of the other parameters were kept constant. Figure 3 shows the SEM images of samples of this experimental series. As we can see in Fig. 3, at simple DC current (without pulse), SnS-SnO2 nanocomposites are small and less uniform. At the frequency of 4 Hz, the agglomerations of particles are seen. At the frequency of 7 Hz (Fig 3c), the nanoparticles are smaller with improper morphology. But as it is seen in Fig. 3d, the nanoparticles are smaller and more uniform than the others at the frequency of 10 Hz. At the frequency of 11 Hz, particle growth and agglomeration rates are more than nucleation rate. At the frequency of 15 Hz, particles are connected to each other to make agglomeration bulks. Therefore the frequency of 13 Hz is more efficient to obtain suitable morphology and more uniform nanoparticles (Fig. 3f) so particle growth and nucleation processes are equivalent and 141 nm average particle diameters can be achieved.

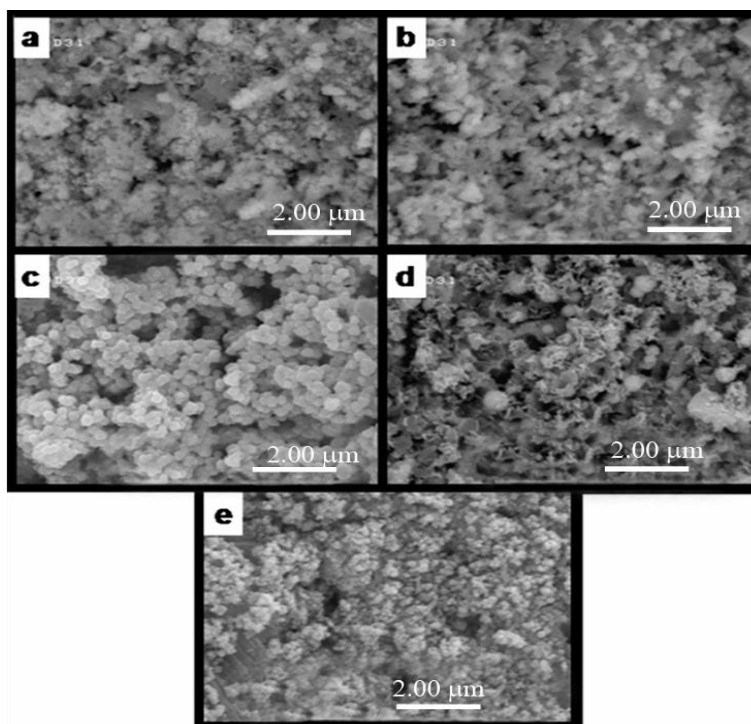## 3.3. Effect of pH solution



**Figure 4.** SEM images of samples with different pHs; 8.5 (a), 10.5 (b), 12.5 (c), 13.5 (d) and 14.5 (e).

For this propose, five samples were synthesized at pHs of 8.5, 10.5, 12.5, 13.5, and 14.5 by adding NaOH while the other parameters were kept constant.

Figure 4 indicates that at pHs of 8.5, 10.5, and 13.5, the synthesized nanoparticles make agglomerations with porous structures due to the releasing of $H_2S$. Solution pH of 14.5 makes smaller and uniform nanoparticles but formation of $SnO_2$ instead of SnS is more probable. Based on the obtained results, at pH solution of 12.5, particle growth and nucleation rates are equivalent, so, 12.5 is suitable pH to synthesize uniform SnS-$SnO_2$ nanoparticles with the average particle sizes of 161 nm.

### 3.4. Optimization of sodium sulfide concentration

To investigate the effects of sodium sulfide concentration on the morphology and particles sizes of the synthesized SnS nanoparticles, we varied the amount of this parameter from 0.24 to $8 \times 10^{-4}$ M while the amounts of the other parameters were kept constant. Figure 5 shows the SEM images of SnS samples that synthesized at different sodium sulfide concentrations.
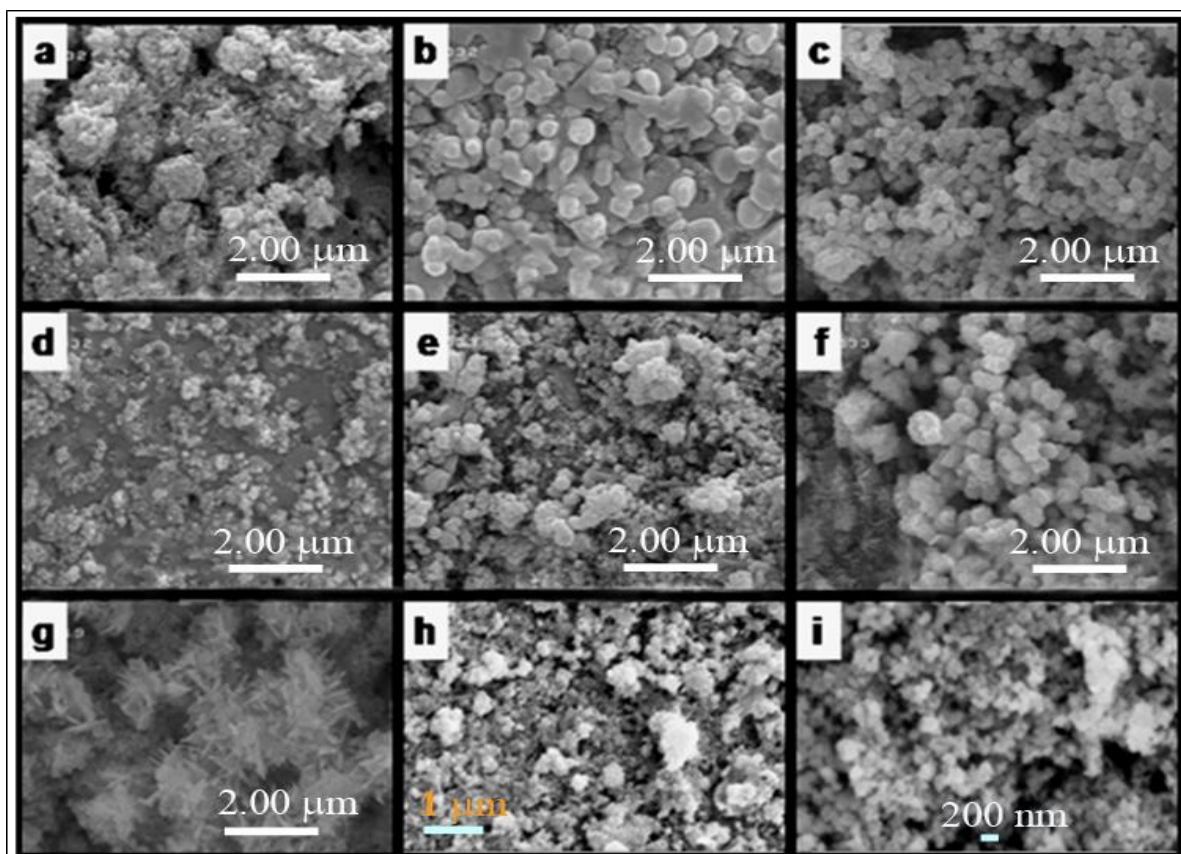


**Figure 5.** SEM images of tin sulfide samples synthesized at different concentrations of sodium sulfide; 0.24 M (a), 0.16 M (b), 0.08 M (c), 0.04 M (d), 0.02 M (e), 0.008 M (f), 0.004 M (g), 0.003 M (h), and $8 \times 10^{-4}$ M (i). The other experimental conditions were kept constant.

The SEM images in Fig. 5 indicate that any decrease in sodium sulfide concentration causes a formation of uniform SnS nanoparticles in spite of performing the synthesis in high voltages and decreasing the number of ions. According to the XRD results, tin sulfide content of the sample synthesized in 0.008 M sodium sulfide is the most (63.02 %wt) therefore 0.008 M is optimum concentration for further studies but 0.004 M makes more uniform nanoparticles with angular and aciform structures, so structurally, 0.004 M of sodium sulfide concentration can selected as optimum value.
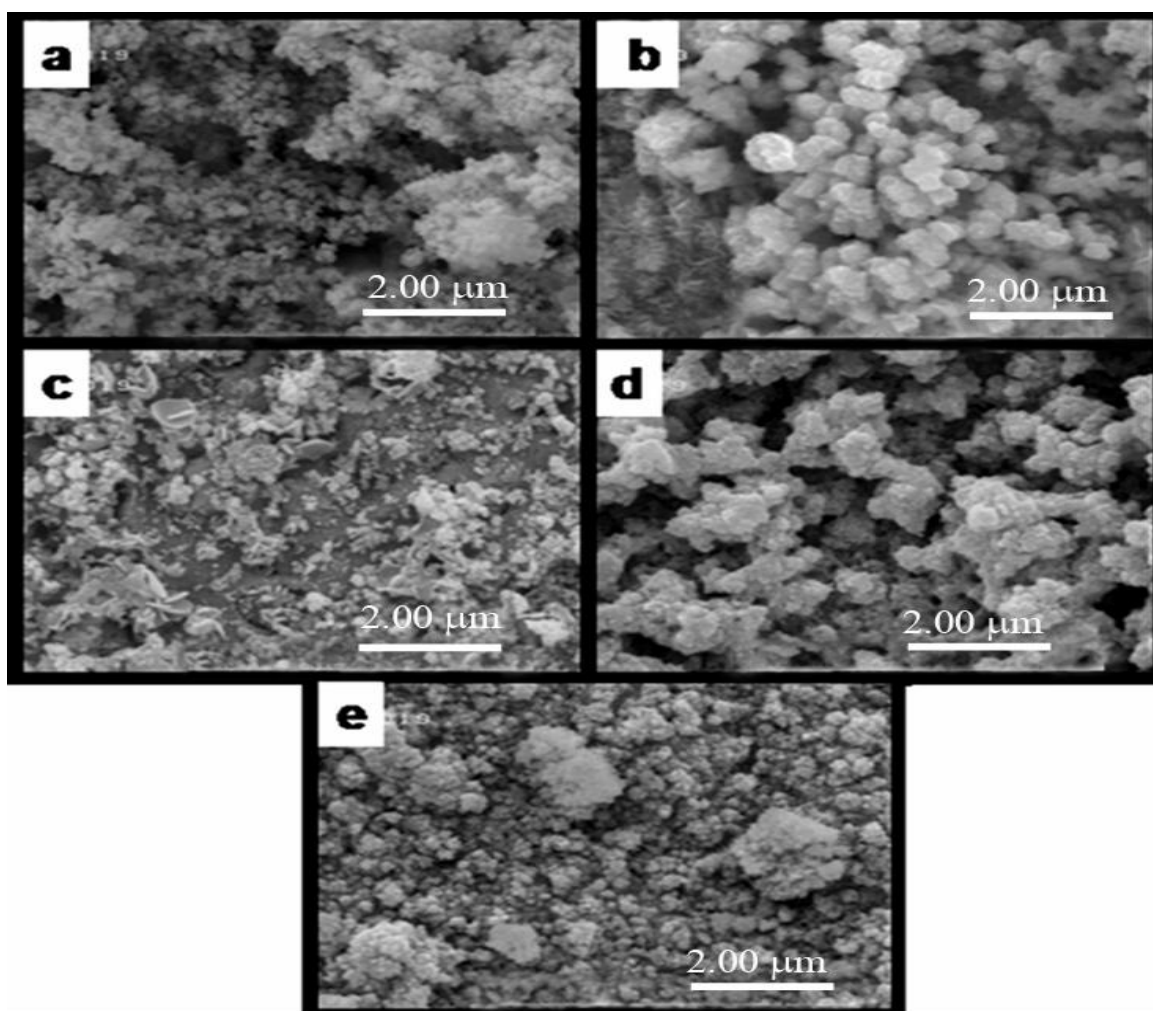
### 3.5. Effect of synthesis temperature



**Figure 6.** SEM images of tin sulfide samples synthesized at temperatures of 0 ℃ (a), 25 ℃ (b), 45 ℃ (c), 75 ℃ (d), and 95 ℃ (e).

Among the synthesis parameters, solution temperature has more effect on the phase composition of the SnS samples and rate constant of reaction is dependent to it. To study the effects of temperatures, five samples were synthesized at different temperatures while amounts of the other parameters were kept constant. The prepared samples were characterized by SEM. Figure 6 shows SEM images of the SnS samples, which synthesized at 0, 25, 45, 75, and 90 °C. As the SEM images

show, the rate of SnS formation is controlled via dissociation of sulfide ions. Therefore, in low temperature due to freezing of these ions, the rate of precipitate formation is slow and consequently, the SnS nanoparticles have unsuitable structures and morphology.
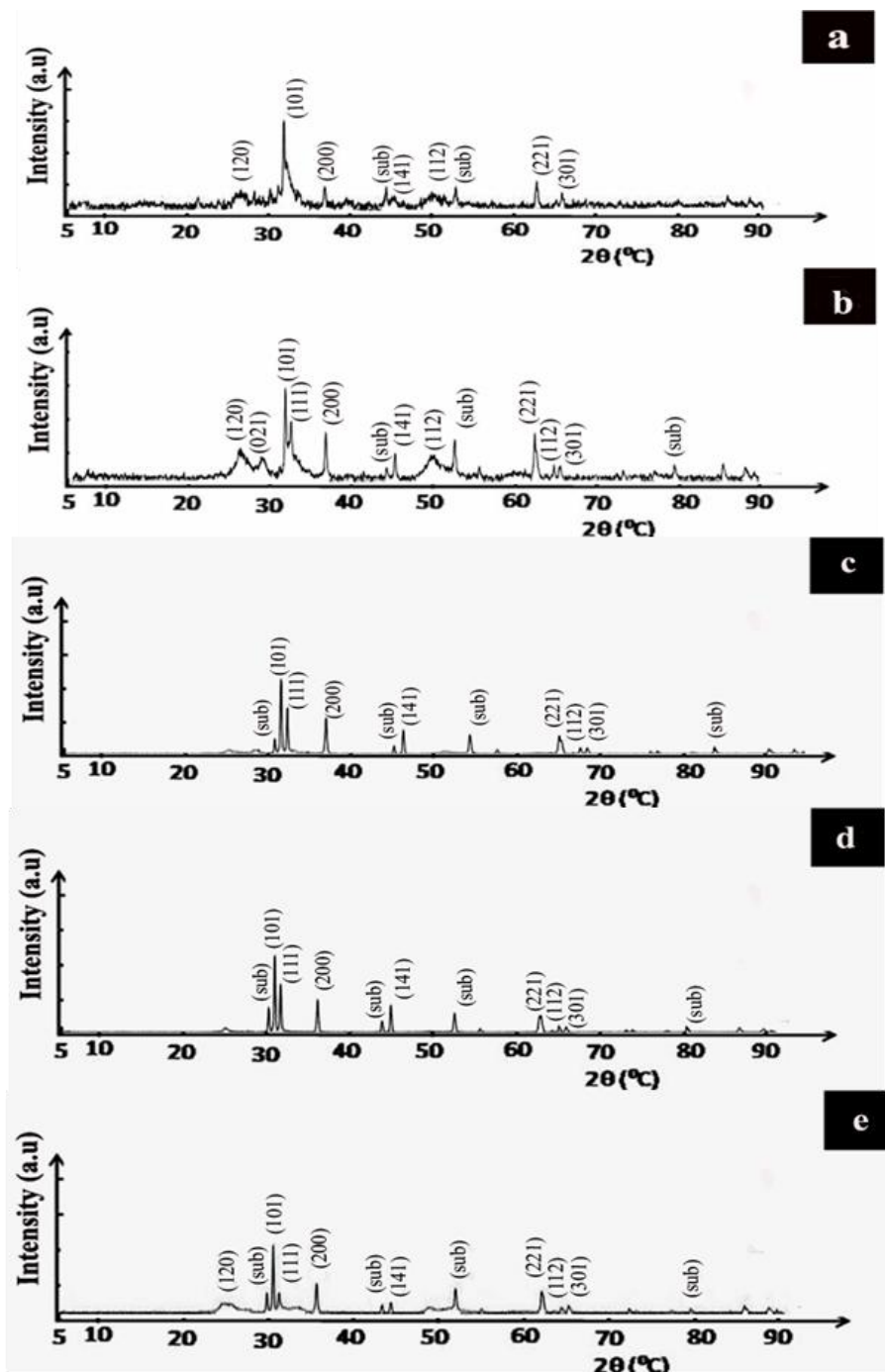


**Figure 7.** XRD patterns of the samples which synthesized at different temperatures of 0 ºC (a), 25 ºC (b), 45 ºC (c), 75 ºC (d), and 95 ºC (e).

When the electrosynthesis is performed at higher temperatures (higher than 25 °C), formation of $SnO_2$ is more probable than SnS. Based on the obtained results, temperature of 25 ºC due to formation of uniform SnS-$SnO_2$ nanocomposites with nanorod structure (Fig. 6b) was selected as

optimum value for the synthesis of the samples. As it is seen in Fig. 6b, the major part of the image includes concrete and hunk structures. In fact, these collections include many adherent nanorods. In the lower left corner of Fig. 6b, the nanorods are seen as separate and apart components.

For further study about the effect of temperature, the samples were analyzed by XRD. Figure 7 shows the XRD patterns of these samples at different temperatures. As it is seen in this figure, at all of these temperatures, tin oxide and pure metallic tin can be seen as well as tin sulfide. In the presented method, the samples are synthesized by direct oxidation of tin anode so it is expected that the samples don't include any metallic tin impurity.

The observed patterns for metallic tin in Fig. 7 are due to this fact that the X-ray can transmit from the synthesized layer and reach to the bed of the electrode. The summary of XRD data are presented in Table 1. It should be mentioned the amounts of metallic tin in all samples were mathematically diffracted and the weight percentages of the others compounds were recalculated.

**Table 1.** Summary of phase analysis based on XRD patterns for samples synthesized at different temperatures

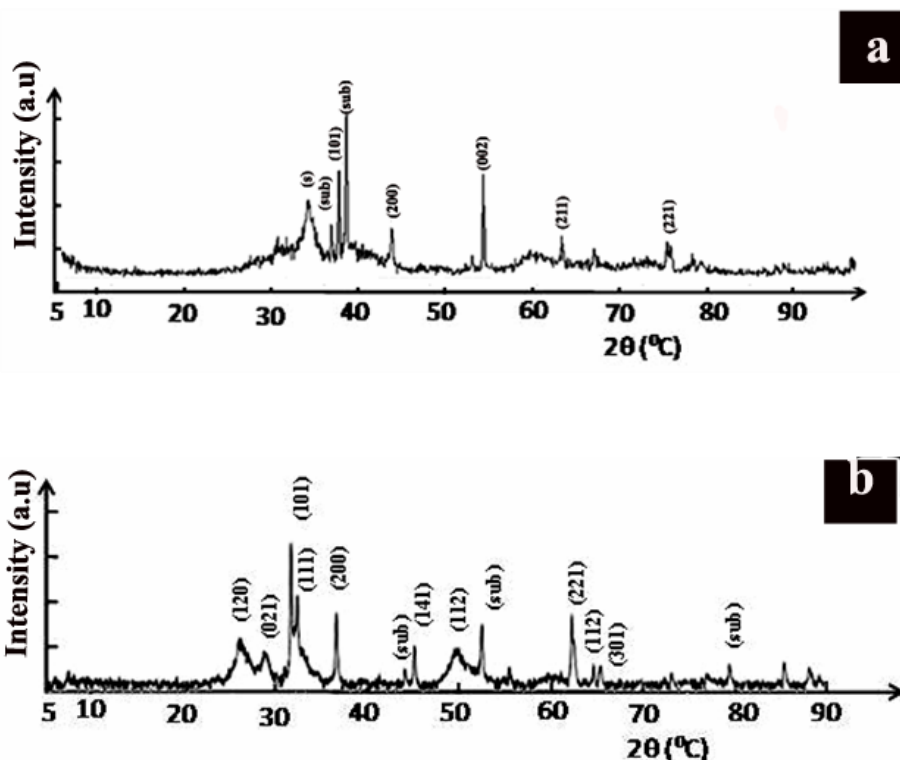| | Samples | | | | |
|---|---|---|---|---|---|
| Compound | a (0 °C) | b (25 °C) | c (45 °C) | d (75 °C) | e (95 °C) |
| $SnO_2$ | 42 | 37 | 63 | 75 | 74 |
| SnS | 58 | 63 | 37 | 25 | 24 |



**Figure 8.** XRD patterns for the samples which synthesized at temperature of 25 °C with 0.008 M sodium sulfide (a), 25 °C with 0.004 M sodium sulfide (b). The other experiment conditions including pulse height, pulse frequency and solution pH were kept constant.

Based on XRD results, the obtained crystals are orthorhombic and also tin sulfide content of samples is decreased when the synthesis temperature is increased from 25 °C up to 95 °C. At temperature of 25 ºC, the sample has the most tin sulfide content (63 %wt). Combining of SEM and XRD results with temperature studies shows that the sample synthesized at 25 °C has uniform morphology with aciform structure and lower impurity. It is possible that the results of this section lead the authors to think the amount of tin sulfide in the samples is also depend on sulfide ion concentration in the synthesis solution. Therefore, two samples were synthesized at 25 °C while sodium sulfide concentration was different (0.008 M and 0.004). Figure 8 shows the XRD patterns of these samples. Based on XRD patterns, the sample synthesized in 0.008 M sodium sulfide include 63 %wt tin sulfide and the sample synthesized in 0.004 M sodium sulfide include 35 %wt tin sulfide. It shows that the value of 0.008 M for sodium sulfide is correctly selected as optimum value.

### 3.6. Effect of additive type

Based on the previous reports, some compounds such as sodium dodecyl sulfate (SDS), polyvinyl pyrrolidone (PVP), glycerol, cetyltrimethyl ammonium bromide (CTAB), saccharin, and diethyl sulfosuccinate (DES) [65-67] have been used as structure director to obtain more uniform nanostructures in nano-scale synthesis to control the mechanism and kinetics of the reactions. In this study, the effects of PVP, SDS, glycerol, and CTAB was investigated on the morphology and particles sizes of the samples, and the amounts of the other parameters of synthesis were kept constant (Fig. 9). As we can see in Fig. 9, additives have no significant effect on the improvement of morphology or particles sizes.
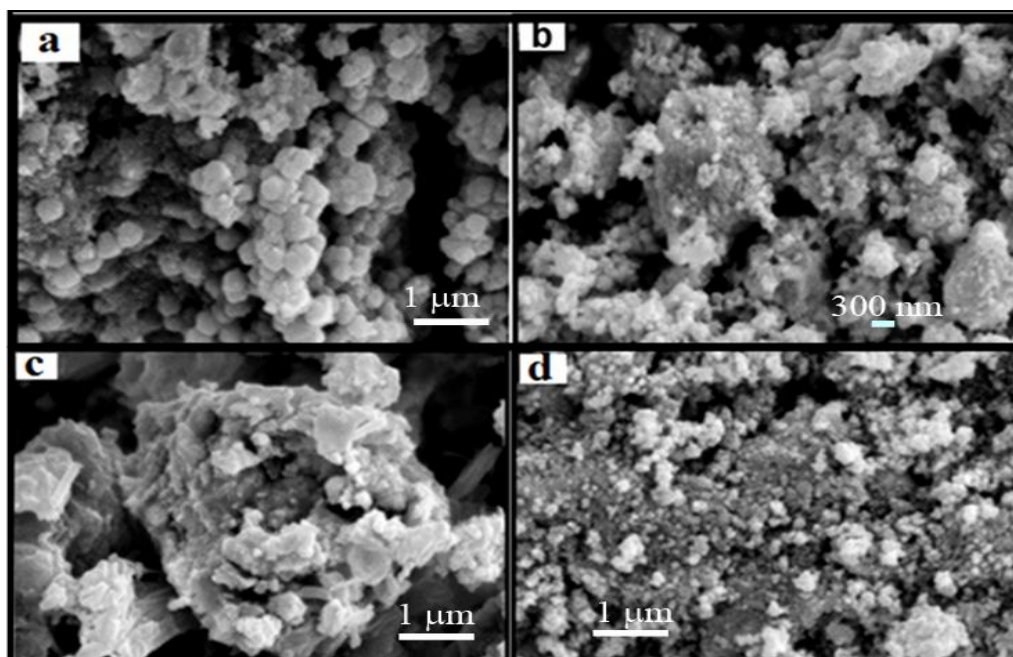


**Figure 9.** SEM images of samples which synthesized in the presence of PVP (a), SDS (b), Glycerol (c), and CTAB (d). The 0.5 % concentration of each additive was used.

To recognize the structure and the properties of the synthesized sample in optimized conditions, it was characterized by TEM and Energy Dispersive X-ray (EDX). Figure 10 indicates the SEM and TEM image of the $SnS$-$SnO_2$ nanorods under a magnification of 60000. Based on the TEM and SEM image, in the optimum conditions, uniform SnS nanorods with 30 average lengths and 200 nm average diameters were synthesized.
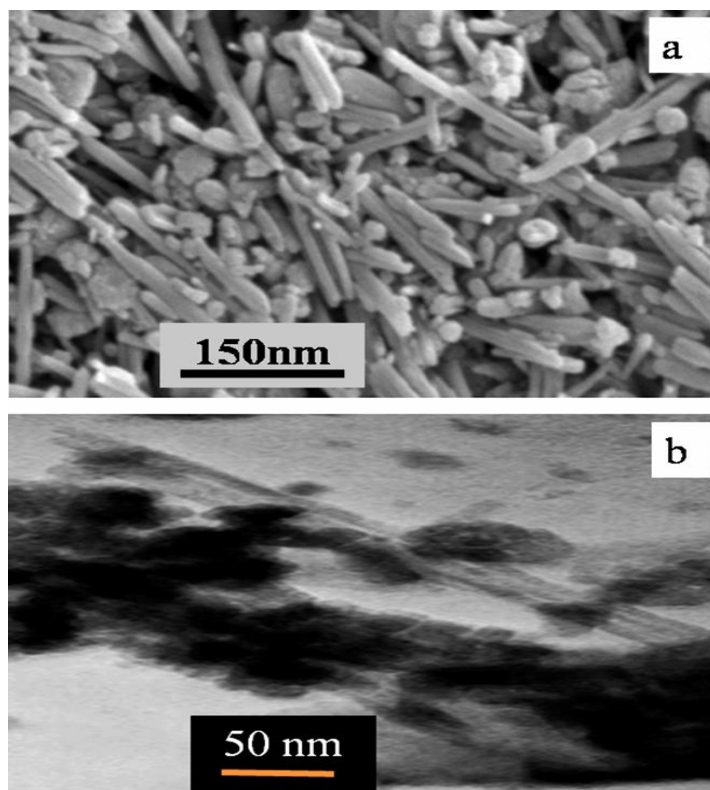


**Figure 10**. SEM image with 30000 magnification (a)**,** and TEM image with 60000 magnification (b) of the optimized SnS nanorods.
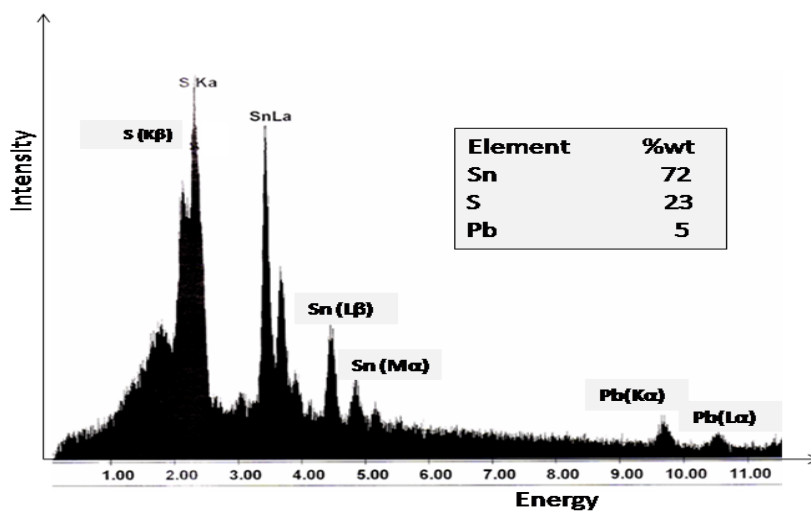


**Figure 11.** EDX patterns for SnS sample which synthesized at 92 mA.cm$^{-2}$ current density, 13 Hz pulse frequency, 0.008 M sodium sulfide, solution pH of 12.5, electrocrystallization temperature of 25 °C.

The EDX patterns of the sample prove that the sample comprises sulfur and tin elements with lead impurity from bed of the electrode (Fig. 11).

## 4. CONCLUSIONS

Pulsed- current electrochemical method can be used as a confident and controllable method to prepare tin sulfide/tin dioxide nanocomposites on the surface of tin electrode, from a basic sodium sulfide solution. In this method, sodium sulfide concentration, concentration of synthesis additive, pH, bath temperature, pulse frequency, and pulse height (current amount) are effective parameters that can change the morphology and the particles sizes of nanocomposite samples.

## References

1. E. Manova, T. Tsoncheva, D. Paneva, I. Mitov, K. Tenchev, L. Petrov, *Appl. Catal. A: Gen* 277 (2004) 119-127.
2. Mao-Sung Wu, Pin-Chi J. Chiang, Jyh-Tsung Lee, Jung-Cheng Lin, *J. Phys. Chem*. B 109 (2005) 23279–23284.
3. L. Carbone, S. Kudera, E. Carlino, W. J. Parak, C. Giannini, R. Cingolani, L. Manna, *J. Am. Chem. Soc.* 128 (2006) 748-755.
4. M. Regragui, M. Addou, A. Outzourhit, J. C. Bernede, E. E. Idrissi, E. Benseddik, A. Kachiuane, *Thin Solid Films* 358 (2000) 40-45.
5. J. Xie, X. Cao, J. Li, H. Zhan, Y. Xia, Y. Zhou, *Ultrason. Sonochem.* 12 (2005) 289-293.
6. Kh. Ghanbari, M. F. Mousavi, M. Shamsipur, *Electrochim. Acta* 52 (2006) 1514-1522.
7. M. Zhoua, S. Chena, S. Zhaoa, H. Ma, *Physica* E 33 (2006) 28-34.
8. A. Curulli, F. Valentini, S. Orlanducci, M. L. Terranova, C. Paoletti, G. Palleschi, *Sens. Actuators* B 100 (2004) 65-71.
9. O. Buriez, I. Kazmierski, J. Pe´richon, *Electroanal. Chem*. 537 (2002) 119-123.
10. E. Perre, L. Nyholm, T. Gustafsson, P. L. Taberna, P. Simon, K. Edström, *Electrochem. Commun.* 10 (2008) 1467-1470.
11. S. C. Tang, X. K. Meng, S. Vongehr, *Electrochem. Commun.* 11 (2009) 867-870.
12. H. Antonya, A. Labrit, J. C. Rouchaud, L. Legrand, A. Chausse, *Electrochim. Acta* 53 (2008) 7173-7181.
13. M. A. Del Valle, M. Gacitúa, F. R. Díaz, F. Armijo, R. del Río, *Electrochem. Commun*. 11 (2009) 2117-2120.
14. N. Cioffi, L. Torsi, L. Sabbatini P. G. Zambonin, T. Bleve-Zacheo, *Electroanal. Chem*. 488 (2000) 42-47.
15. C. A. moina, M. Vazdar, *Electrochem. Commun*. 3 (2001) 159-163.
16. P. Bocchetta, M. Santamaria, F. Di Quarto, *Electrochem. Commun*. 9 (2007) 683-688.
17. M. Lai, D. Jason Riley, *J. Coll. Interface Sci*. 323 (2008) 203-212.
18. S. Ghasemi, H. Karami, M. F. Mousavi, M Shamsipur, *Electrochem. Commun*. 7 (2005) 1257-1264.
19. L. M. Chang, M. Z. An, H. F. Guo, S. Y. Shi, *Appl. Surf. Sci*. 253 (2006) 2132-2137.

20. P. Gyftou, E. A. Pavlatou, N. Spyrellis, *Appl. Surf. Sci*. 254 (2008) 5910-5916.
21. N. S. Qu, K. C. Chan, D. Zhu, *Scripta Materialia* 50 (2004) 1131-1134.
22. M. Ma, V. S. Donepudi, G. Sandib, Y. K. Sunc, J. Prakash, *Electrochim. Acta* 49 (2004) 4411-4416.
23. H. H. Zhoua, S. Q. Jiaoa, J. H. Chenb, W. Z. Weib, Y. F. Kuanga , *Thin Solid Film*. 450 (2004) 233-239.
24. H. Adelkhani, M. Gaemi, *Solid State Ion*. 179 (2008) 2278-2283.
25. L. M. Chang, M. Z. An, H. F. Guo, S. Y. Shi, *Appl. Surf. Sci*. 253 (2006) 2132-2137.
26. P. Gyftou, E. A. Pavlatou, N. Spyrellis, *Appl. Surf. Sci*. 254 (2008) 5910-5916.
27. S. Y. Hong, R. Povitz, Y. Prior, R. Tenne, *J. Am. Chem. Soc*. 125 (2003) 10470-10476.
28. A. L. Rogach, A. Eychmuller, S. G. Hickey, S. V. Kershaw, *Small* 3 (2007) 536-739.
29. J. M. Luther, M. C. Beard, Q. Song, M. Law, R. J. Ellingson, A. Nozik, *J. Nano. Lett*. 7 (2007) 1779-1784.
30. D. V. Talapin, C. B. Murray, *Science* 310 (2005) 86-91.
31. N. Petkov, J. Xu, M. A. Morris, J. D. Holmes, *J. Phys. Chem*. C 112 (2008) 7345-7349.
32. K. Jiang, Y. Wang, J. Dong, L. Gui, Y.Tang, *Langmuir* 17(2001) 3635-3639.
33. T. Kim, D. Son, M. Choi, B. Parc, *J. Power Sources* 167 (2007) 529-533.
34. J. Seo, J. Jang, S. Park, C. Kim, B. Park, J. Chon, *Adv. Mater* 20 (2008) 4269-4275.
35. S. K. Panda, A. Datta, A. Dev, S. Gorai, S. Chaudhuri, *Crystal Growth* 6 (2006) 2177-2182.
36. S. Vaucher, M. Li, S. Mann, *Angew. Int*. Ed. 39 (2000) 1793-1799.
37. Z. Y. Zhong, Y. D. Yin, B. Gates, Y. N. Xia, *Adv. Mater*. 12 (2000) 206-211.
38. S. Boonsalee, R. W. Gudavarthy, J. A. Bohannan, *Chem. Mater*. 20 (2008) 5737-5742.
39. S. Cheng, G. Chen, Y. Chen, C. Huang, *Opt. Mater*. 29 (2006) 439-444.
40. L. R. Bohannan, E. W. Switzer, G. A. Oba, *Appl. Phys. Letters* 83 (2003) 1944-1952.
41. J. Kang, J. Park, D. Kim, *Electrochem. Commun*. 12 (2010) 307-310.
42. H. Hu, B. Yang, J. Zeng, Y. Qing, *Mat. Phys*. 86 (2008) 233-239.
43. L. S. Price, I. P. Parking, A. M. E. Hardy, R. Clark, *Chem. Mater*. 11 (1999) 1792-1799.
44. T. Jiang, G. A. Ozin, *J. Mat. Chem*. 8 (1998) 1099-1108.
45. B. Polosz, W. Steurer, H. Schulz, *Acta Crystallogr. Sect*. B 46 (1990) 449-455.
46. A. Ortiza, J. C. Alonso, M. Garcia, J. Toriz, *Semicond. Sci. Technol*. 11 (1996) 243-249.
47. I. P. Parking, A. T. Rowley, *Polyhedron* 12 (1993) 2961-2968.
48. A. Ortiz, S. Lopez, *Semicond. Sci. Technol*. 9 (1994) 2130-2136.
49. P. Bilijana, G. Lavan, T. Atanas, *Chem. Phys*. 83 (2004) 245-249.
50. M. M. Elnahass, H. M. Zeyada, *Opt. Mater*. 20 (2002) 159-165.
51. L. Sato, M. Ichimura, E. Aria, Y. Yamazaki, *Sol. Eng. Mater. Sol. Cell* 85 (2005) 153-157.
52. Y. Liu, D. Hou, G. Wang, *Chem. Phys. Lett*. 379 (2003) 67-72.
53. G. H. Yue, D. L. Peng, P. X. Yan, *J. Alloy. Compd*. 468 (2009) 254-258.
54. Y. Wang, H. Gong, B. Fan, G. Hu, *J. Phys*. C 114 (2010) 3256-3264.
55. D. Giri, K. K. Das, *J. Phys*. A 109 (2005) 7207-7212.
56. B. J. Seo, J. Jang, S. Park, C. Kim, B. Park, *Adv. Mater*. 20 (2008) 4269-4275.
57. J. Huang, K. Yu, C. Gu, M. Zhai, Y. Wu, M. Yang, J. Liu, *Sens. Actuators* B 147 (2010) 467-474.
58. K. Choi, J. Park, K. Park, H. Kim, H. Park, S. Kim, *Sens. Actuators* B 150 (2010) 65-72.
59. Y. Zhao, Z. Zhang, H. Dang, W. Liu, *Mater. Sci. Eng*. B 113 (2004) 175-178.
60. E. Comini, G. Faglia, G. Sberveglieri, Z. Pan, Z.L. Wang, *Appl. Phys. Lett*. 81 (2002) 1869-1871.
61. X. Kong, Y. Li, *Sens. Actuators* B 105 (2005) 449-453.
62. E. Comini, *Analytica Chimica Acta* 568 (2006) 28-40.
63. H. Karami and O. Rostami-Ostadkalayeh, *J. Clust. Sci*. 20 (2009) 587-600.
64. H. Karami, S. Mohammadi, *J. Cluster. Sci*. 21, 4 ( 2010) 739-752.
65. J. Lee, T. Isob, M. Senna, *Colloid Interface Sci*. 177 (1996) 490-494.

66. C. W. Kwon, T.S Yoon, S. S. Yim, S. H. Park and K. B. Kim, *J. Nanopart. Res*. 11 (2009) 831-839.
67. Z. Y. Yuan, T. Re and B. L. Su, *J. Catalysis Today* 95 (2004) 743-750.